Association of Cytochrome *c* with Membrane-Bound Cytochrome *c* Oxidase Proceeds Parallel to the Membrane Rather Than in Bulk Solution

Alexander Spaar,[†‡] Dagmar Flöck,[§] and Volkhard Helms[†*]
[†]Center for Bioinformatics, Saarland University, Im Stadtwald, Saarbrücken, Germany; [‡]Department of Cell Biology and Oncology, Consorzio Mario Negri Sud, Santa Maria Imbaro (Chieti), Italy; and [§]Department of Chemistry, University of Rome "La Sapienza", Rome, Italy

ABSTRACT Electron transfer between the water-soluble cytochrome *c* and the integral membrane protein cytochrome *c* oxidase (COX) is the terminal reaction in the respiratory chain. The first step in this reaction is the diffusional association of cytochrome *c* toward COX, and it is still not completely clear whether cytochrome *c* diffuses in the bulk solution while encountering COX, or whether it prefers to diffuse laterally on the membrane surface. This is a rather crucial question, since in the latter case the association would be strongly dependent on the lipid composition and the presence of additional membrane proteins. We applied Brownian dynamics simulations to investigate the effect of an atomistically modeled dipalmitoyl phosphatidylcholine membrane on the association behavior of cytochrome *c* toward COX from *Paracoccus denitrificans.* We studied the negatively charged, physiological electron-transfer partner of COX, cytochrome c_{552}, and the positively charged horse-heart cytochrome *c*. As expected, both cytochrome *c* species prefer diffusion in bulk solution while associating toward COX embedded in a membrane, where the partial charges of the lipids were switched off, and the corresponding optimal association pathways largely overlap with the association toward fully solvated COX. Remarkably, after switching on the lipid partial charges, both cytochrome *c* species were strongly attracted by the inhomogeneous charge distribution caused by the zwitterionic lipid headgroups. This effect is particularly enhanced for horse-heart cytochrome *c* and is stronger at lower ionic strength. We therefore conclude that in the presence of a polar or even a charged membrane, cytochrome *c* diffuses laterally rather than in three dimensions.

INTRODUCTION

The electron transfer between the water-soluble electron carrier cytochrome *c* and the integral membrane protein cytochrome *c* oxidase (COX) is a primary event in biological energy transduction in the mitochondrial inner membrane and the cytoplasmic membrane of many bacteria. COX has four redox active sites, the Cu_A center, which is close to the Trp^{121} electron entry site, heme *a*, and the binuclear heme a_3/Cu_B site of O_2 reduction (1–3). These redox reactions, which lead to reduction of dioxygen to water, are coupled to proton translocation across the membrane, and the resulting electrochemical proton gradient can drive reactions such as the synthesis of ATP from ADP (4).

In this study, we focus on the first step of this reaction, the diffusional association of cytochrome *c* toward COX. This process is dominated by the long-range electrostatic attraction between the two proteins, and possibly between cytochrome *c* and the membrane. The endpoint of the diffusional association is the formation of the encounter complex, which is a state where the proteins have oriented their interaction patches to facilitate the formation of the bound complex. For the amino-terminal domain of enzyme I and the phosphocarrier protein HPr, Tang and co-workers recently were able to visualize the distribution of encounter complexes by paramagnetic relaxation enhancement in combination with restrained simulated annealing (5).

To study the diffusion-controlled part of the association, we performed Brownian dynamics (BD) simulations, which have become a powerful method for the computational analysis of the kinetics of protein-protein interactions (6–8). We used the crystal structures of the soluble fragment of cytochrome c_{552} (cyt c_{552}) and COX, both from *Paracoccus denitrificans*, and horse-heart cytochrome *c* (cyt c_h). Ludwig et al. previously examined the electron transfer rates for soluble fragments of cyt c_{552} and of the Cu_A domain of COX (also from *P. denitrificans*), and for cyt c_h and COX at varying ionic strength and with different mutations (9,10). They found a strong dependence of the rates on the ionic strength, indicating a dominant role of the electrostatic interaction in the association behavior, and making the technique of BD simulations particularly suitable for studying this system (11). The modeling of the subsequent binding process requires more detailed simulation techniques, such as steered molecular dynamics simulations (12) or, as in the case of electron transfer processes, Franck-Condon factor or Marcus theory approaches. For example, Miyashita and co-workers used several techniques in an integrated fashion to clarify the binding process and the electron transfer between cytochrome c_2 and the photosynthetic reaction center (13–15). Further theoretical studies on the binding of proteins to lipid bilayers (for example) have used Poisson-Boltzmann continuum electrostatics to study a variety of biological processes ranging from phosphoinositide signaling to retroviral assembly (16,17).

A previous study by our group on the cytochrome *c* and COX system (18) focused on the computation of association

Submitted July 31, 2008, and accepted for publication November 10, 2008.

*Correspondence: volkhard.helms@bioinformatik.uni-saarland.de

Editor: Marilyn Gunner.

0006-3495/09/03/1721/12 $2.00

doi: 10.1016/j.bpj.2008.11.052

rates at varying ionic strength and for point mutants using BD simulations. The relative association rates were in good agreement with the electron transfer rates from the experiments. In particular, the effects of ionic strength and protein mutations were qualitatively reproduced. However, the individual association rates were significantly larger than the experimental electron transfer rates, suggesting that only a small fraction of the successful BD trajectories leads to an electron transfer. Since to date there is no crystal structure available for the complex of cyt c_{552}/COX, this previous study (18) used a model of the bound conformation from a preceding docking study (19) to define the endpoint of successful BD association trajectories. However, a subsequent NMR study that measured the chemical shifts of cyt c_{552} residues in the free form and in the complex with COX showed some disagreements with this docked complex (20,21). A later protein-protein docking study that included the NMR distance restraints during the docking stage showed that no single static structure could simultaneously satisfy all of the experimental data (22). The bound complex must therefore instead exist as a dynamic ensemble of different orientations. Moreover, the docked complex may well be another intermediate before the tightly bound complex is formed in which the electrons can be transferred to COX. We note that the uncertainty about the conformation of the bound state does not affect the interpretation of the results from this study, where we focus on the association pathways toward the encounter-state ensemble.

In this study, we investigated two of the most interesting aspects in the association of cytochrome *c* with COX, preceding the formation of the bound complex. These are the role of the membrane and the effects of the different redox states on the association behavior of this electron-transfer system. More precisely, we focused our attention on the following questions: 1), Does a focused encounter complex exist? 2), What is the effect of the membrane on the diffusional behavior of cytochrome *c*? 3), Is the association behavior different for the two cytochrome *c* species? and 4), What are the effects of the different redox states? Currently, there exist two competing models for the association of cytochrome *c* with COX: either the diffusion is described as a three-dimensional Brownian motion in the bulk solvent that is only affected by the electrostatic interaction between the proteins, or the diffusion is pictured as proceeding in two dimensions along the membrane surface (23,24). Gorba et al. have used BD simulations with simplified dipolar sphere-models to characterize the concentration profiles at surfaces of varying net charge (25). For surfaces with a 100% ratio of negatively charged lipids, they found a surface concentration almost 20 fold higher than that in the bulk. The latter scenario would coincide well with the relatively close vicinity of the electron entry site (Trp^{121}) on the COX surface to the membrane surface. This distance of ~10 Å merely allows cytochrome *c* to bind without penetrating the membrane. On the other hand, diffusion along the membrane surface restricts the motional degrees of freedom, which could either favor binding by preorientating the cytochrome *c* molecules, or be entropically unfavorable.

To find a clear answer to the above stated questions, it was necessary to examine the association pathways of cytochrome *c* by following the individual trajectories of the proteins. Recently, we have introduced a method for analyzing the trajectories during BD simulations (26) by extending the simulation of diffusional association of proteins (SDA) program (6). The extended program was previously applied to the analysis of the association of barnase and barstar to calculate the underlying entropy and free-energy landscape, the encounter complex regions, and the optimal association pathways (27). In this study, these novel analysis tools are now applied to the characterization of the association pathways and free-energy landscape for the interaction of two cytochrome *c* species with COX embedded in an atomistically modeled large square dipalmitoyl phosphatidylcholine (DPPC) membrane patch.

MATERIALS AND METHODS

Protein structures

The coordinates of the two-subunit COX, the soluble fragment of cyt c_{552}, and cyt c_h were taken from the Protein Data Bank (PDB codes 1ar1 for COX (28), 1ql3 for cyt c_{552} (29), and 1hrc for cyt c_h (30)) and used as described in Flöck and Helms (18). One focus of this study was to investigate the association behavior of cyt c_h and cyt c_{552} with COX for different redox states. COX has four reduction sites: the two hemes (heme *a* and heme a_3) and the two copper centers (Cu_A and Cu_B). The charges of these sites in the reduced (oxidized) states were assumed to be −2 e (−1 e) for the hemes, +1.0 e (+1.5 e) for each of the copper atoms of Cu_A, and +1 e (+2 e) for Cu_B. The total charge of COX is −7 e in the fully oxidized state and −11 e in the fully reduced state, where we neglected possible changes in the protonation states of titratable residues upon reduction (31). Assigning neutral histidine residues resulted in a total charge of +8 e for oxidized cyt c_h, and of −2 e for oxidized cyt c_{552}.

The membrane patch used in the simulations was constructed by assembling eight squared patches of pure lipid membrane and one central membrane patch of the same size with the COX embedded, resulting in a square membrane patch with dimensions of ~225 Å and containing more than 200,000 atoms (for more details, see Flöck and Helms (18)). For the simulations with the charged lipid membrane, the nitrogen atoms of the choline headgroups from all lipids were charged with −0.2 e.

Computation of forces

For the modeling of the long-range electrostatic interaction of the proteins, solutions of the full Poisson-Boltzmann equation were computed for each protein using the Adaptive Poisson-Boltzmann Solver program (32). Partial charges and atomic radii were taken from the AMBER force field (33). For cyt c_{552} and cyt c_h, cubic grids were used, with 161 nodes and a 1.0-Å spacing, centered on each of the proteins. For fully solvated COX and membrane-embedded COX, we used cubic grids with 225 nodes and the same spacing. The ionic strength was set to 200 mM and the temperature was set to 298.15 K. The solvent dielectric was assigned a value of 78.5, and the dielectric constant for the protein interior was set to 2.0.

The effective charge method (ECM) (34) was used to derive charges that represent the external electrostatic potential in a uniform dielectric medium. The effective charges were fitted to reproduce the electrostatic potential in

a 3-Å-thick layer, starting at the accessible surface defined by a probe of radius 4 Å and extending outward from the protein. Short-range repulsive forces were treated by an exclusion volume that prohibited van der Waals overlap of the proteins. The exclusion volume was precalculated on a grid with 0.5-Å grid spacing (35).

Charge desolvation penalties were computed in an approximate fashion that treats the solvation of each charge independently (7). The charge desolvation penalty of one protein is taken as the sum of desolvation penalties of each charge of that protein. The desolvation penalty of each charge is the sum of desolvation penalties due to the low dielectric cavity of each atom of the other protein. The desolvation energy of protein 1 due to the presence of protein 2 is approximated as

$$\Delta G_{\mathrm{ds}} = \alpha \frac{\varepsilon_s - \varepsilon_p}{\varepsilon_s(2\varepsilon_s + \varepsilon_p)} \sum_{ij} (1 + \kappa r_{ij})^2 e^{-2\kappa r_{ij}} \frac{q_i^2 a_j^3}{r_{ij}^4},$$

where κ is the Debye-Hückel parameter, ε_s and ε_p are the dielectric constants of the solvent and the protein, respectively, q_i is the effective charge on the ith atom of protein 1, a_j is the radius of the jth atom of protein 2, and r_{ij} is the distance between the two atoms. The summation is carried out over all possible pairs of effective charges on protein 1 and atoms on protein 2. The scaling factor, α, for the weighting between electrostatic interaction and desolvation terms was set to 1.67 (7,18).

For the calculation of association rates for the different redox states, the atom-atom contacts of the reaction patches were assigned in a fully automated way (6). We adopted the same contact pairs for definition of contact formation as in Flöck and Helms (18). Possible contacts are those pairs between hydrogen-bond donor and acceptor atoms that have a separation distance of <5.0 Å in the x-ray structure of the complex.

Brownian dynamics simulations

The BD simulations were performed with the SDA software package (36), which was modified to provide a detailed analysis of the trajectories (26,27). Here, the proteins are modeled as rigid bodies, and short-range interactions such as van der Waals forces, hydrophobic forces, and the formation of hydrogen bonds and salt bridges are not modeled. However, these simplifications become important only at small protein-protein separations.

To obtain a high level of statistics for the occupancy maps, 100,000 trajectories were simulated for each protein pair. As in the previous study (18), the trajectories started with the two proteins at a center-to-center distance b, with randomly chosen orientations in the upper hemisphere with a minimum distance of 20 Å to the membrane, and finished when the proteins reached a center-to-center distance $c > b$. In Flöck and Helms (18), b was chosen as 115 Å and c as 540 Å. In this study, b was set to 200 Å so that the trajectories started outside the range of the energy and occupancy grids that are computed during the simulations. On the other hand, c was decreased to 205 Å, as we were focusing our attention on the analysis of the trajectories and were aiming at a high level of statistics instead of improving the association rates. We note that the sphere of radius b is about twice as large as the central membrane patch. This allows the diffusing cyt c_{h} to explore all regions of space on both sides of the membrane patch. One can therefore apply the same rate formalism for computation of association rates, k_{on}, from the SDA trajectories as for normal pairs of two proteins as described previously (18,37).

The diffusion equation was solved with the Ermak-McCammon algorithm (38). The translational Brownian motion of two interacting proteins is simulated as the displacement $\Delta\boldsymbol{r}$ of the relative separation vector $\boldsymbol{r}$ during a time step Δt, according to the relation

$$\Delta\boldsymbol{r} = \frac{D\Delta t}{k_{\mathrm{B}}T}\boldsymbol{F} + \boldsymbol{R}, \text{ with } \langle\boldsymbol{R}\rangle = 0 \text{ and } \langle\boldsymbol{R}^2\rangle = 6D\Delta t,$$

where $\boldsymbol{F}$ is the systematic interparticle force, k_{B} is the Boltzmann constant, T is the temperature, and $\boldsymbol{R}$ is the stochastic displacement arising from collisions of the proteins with solvent molecules. Two analogous formulae are used to generate the rotational motions of the two proteins in terms of rotation angle, $\boldsymbol{w}_j = (w_{1j}, w_{2j}, w_{3j})$, torque $\boldsymbol{T}_{ij}$ acting on protein i due to protein j, and rotational diffusion constant D_{iR} of each protein i ($i, j = 1, 2, i \neq j$):

$$\Delta\boldsymbol{w}_i = \frac{D_{iR}\Delta t}{k_{\mathrm{B}}T}\boldsymbol{T}_{ij} + \boldsymbol{W}_i, \text{ with } \langle\boldsymbol{W}_i\rangle = 0 \text{ and } \langle\boldsymbol{W}_i^2\rangle = 6D_{iR}\Delta t.$$

The diffusional properties of the molecules were assumed to be isotropic. For cytochrome c, a translational diffusion constant of 0.015 Å^2/ps was assigned (39), and the rotational diffusion constant was set to 4.0×10^{-5} rad^2/ps. Since COX is an integral transmembrane protein, it was kept fixed in the simulations. The time step was set to 2.0 ps for center-to-center distances of up to 125 Å, and for larger distances it increased linearly with the intermolecular separation. This corresponds to an average random displacement of 0.4 Å at small and medium separations. For the calculation of the average lifetimes of cytochrome c near the membrane, we measured the lifetime in the region $z = 40$–50 Å, and in the region $z = 37$–47 Å for COX embedded in a 20% negatively charged membrane, every time the protein entered this region.

To reduce the computational cost of the simulations, no hydrodynamic interactions were considered. It has been shown that in general these effects on protein-protein association rates are small (40). Also, previous BD studies with simplified cytochrome c molecules have shown that hydrodynamics has only a small influence (25).

Computation of the occupancy landscape

The analysis of the trajectories with the aim of computing the occupancy maps, the entropy, and the free-energy landscape is described in detail by Spaar and Helms (26). After each time step of the simulated trajectories, the positional and orientational coordinates of protein 2 (relative to protein 1) are computed with respect to a reference coordinate system. During the simulations, these coordinates are assigned to the nodes of a six-dimensional grid on which the occupancy, energy, and entropy maps are computed.

The computation of the occupancy maps with respect to the positional coordinates can be interpreted as projecting the position of protein 2 onto a plane that is perpendicular to the center-to-center vector of the proteins in the bound state of the crystal structure. A spherical coordinate system was used, θ and ϕ denoting the corresponding polar and azimuthal angles between the center-to-center vector of the proteins at a trajectory position and the center-to-center vector of the proteins in the bound state. Since the maps are computed with respect to a "semi-Cartesian" coordinate system, the axes are called ϕ_x and ϕ_y, which are the x and y components of the angle ϕ. The occupancy maps with respect to the orientational coordinates are computed in the same way. The normal vector of the interaction patch of protein 2 is projected onto a plane that is perpendicular to the normal vector of the interaction patch of protein 1. The axes are $\phi_{n,x}$ and $\phi_{n,y}$, according to the azimuthal angle ϕ_n between the normal vector of the interaction patch of protein 2 and that of protein 1. The index n refers to the normal vectors of the reaction patches.

The electrostatic and desolvation energies, and the translational and rotational entropy losses (see below), are recorded in further sets of matrices (not shown). In the matrices assigned to the electrostatic and desolvation energies, the minimum values for the given position/orientation are stored, thus allowing the final identification of the minimum free-energy paths. Along the angles ϕ_x and ϕ_y, and $\phi_{n,x}$ and $\phi_{n,y}$, we used a discretization with 101 nodes, i.e., an average step size of 1.8°. Along the distance axis, $d_{1\text{-}2}$, a spacing of 2 Å was used over a distance of 80 Å. The initial value was set by the center-to-center distance between the proteins in the bound state. Finally, the occupancy values are normalized according to the volume of the corresponding element of the configuration space.

Calculation of the entropy landscape

By interpreting the computed occupancy maps as probability distributions, the contribution of the translational and rotational entropy to the free energy landscape is computed from the restriction of the degrees of motional freedom and by applying a local entropy function. The total entropy loss of the protein-protein encounter is approximated as the sum of the translational and rotational entropies $\Delta S = \Delta S_{\mathrm{trans}} + \Delta S_{\mathrm{rot}}$. Since the proteins are simulated as rigid bodies, we do not account for changes of the internal entropy of the proteins resulting from vibrational modes and side-chain conformations.

The process of protein encounter is considered as a step-by-step process at a molecular level, where we analyze whether a protein at a certain position and with a certain orientation can explore the full configuration space within a Brownian Dynamics time step. In this way, we characterized the position- and orientation-dependent (local) entropy loss, rather than the global entropy loss during the association process, which can be computed using the Sackur-tetrode equation (41). For the computation of the local entropy loss, we only take into account the occupancy values of all those configurations (positions and orientations) that are reachable from the particular position and orientation which are within its accessible volume of the configuration space (i.e., within one Brownian dynamics time step). The accessible spatial and angular volumes V and Y are defined as spheres around the current position of the protein, and around its current orientation. The corresponding radii are $\Delta\rho = 3$ Å and $\Delta\omega = 3^{\circ}$, respectively. To compute the local entropy loss at the given position and orientation from the occupancy of the positions and orientations (the states) within the accessible volumes V and Y, the occupancy landscape is interpreted as a probability distribution, which allows the application of the basic entropy formula $S = k_B \sum P_n \ln P_n$, where P_n represents the probabilities for each state n. This configuration-dependent entropy value is then compared to the entropy of a constant, isotropic probability distribution, which is the reference state if the proteins are far apart. Note that the entropy loss is computed separately for all of the grid nodes of the positional and orientational space, which together represent the entropy landscape (see Spaar and Helms (26) for details).

Free-energy landscape

With the energy and entropy contributions as functions of the translational and rotational coordinates, the free-energy landscape of the encounter process is computed as the sum of electrostatic energy, desolvation energy, and translational/ rotational entropy:

$$\Delta G = \Delta E_{\mathrm{el}} + \Delta E_{\mathrm{ds}} - T\,\Delta S_{\mathrm{tr}}, \quad \Delta S_{\mathrm{tr}} = \Delta S_{\mathrm{trans}} + \Delta S_{\mathrm{rot}}.$$

The membrane affects the energy profiles along the reaction path, defined as the path along the minima of the free-energy landscape (see Fig. 5), namely, the electrostatic interaction energy ΔE_{el}, the desolvation energy ΔE_{ds}, the (negative) translational and rotational entropy loss, $-T\Delta S$, and the free energy, ΔG, of the protein-protein association.

RESULTS

Brownian dynamics simulations were performed in this study to investigate the association behavior of the electron-transfer-system cytochrome c (cyt c_{h} and cyt c_{552}) toward COX. In particular, we focused on the effects of the membrane and of the different redox states by applying a recently developed methodology (26) to examine and evaluate the conformations and energies along the simulated trajectories.

To study the effect of the membrane, we investigated four different scenarios for cyt c_{h} and cyt c_{552} in association with 1), COX solvated in water; 2), COX embedded in an uncharged membrane; 3), COX embedded in a polar membrane; and 4), uncharged COX embedded in a polar membrane. For the simulations with an uncharged membrane or with uncharged COX, we switched off all the partial charges of the lipids and COX, respectively. Note that DPPC lipids are zwitterionic but without net charge. Further simulations were run to study the association of cytochrome c with COX in the presence of a 20% negatively charged membrane by placing a -0.2 e charge on the choline nitrogen of each lipid. Here, the net charge of -0.2 e per lipid was chosen to mimic the percentage of negatively charged lipids in cellular membranes (42). To study the effect of the ionic strength on the association behavior of cytochrome c, we ran the simulations of the first three scenarios, the association to COX solvated in water, and to COX embedded in an uncharged or polar membrane, at lower ionic strength, 50 mM for cyt c_{552} and 140 mM for cyt c_{h}.

Next, we studied the effect of different redox states resulting from electron transfer from cytochrome c to COX on the free-energy landscape. In this part, we focused on cyt c_{552}, which is the physiological counterpart of COX. Two scenarios were examined: the change in the free-energy landscape due to electron transfer to completely oxidized COX, and the change due to electron transfer to the enzyme oxidized only at the Cu_A center, resulting in a completely reduced COX. Below, we present results first for the membrane effect and then for the effects of the redox state.

Effects of the membrane

The central piece of the membrane used in the simulations is a single snapshot of a molecular dynamics simulation of COX embedded in a DPPC membrane, which was extended with identical patches of pure lipid membranes to create a square membrane with side dimensions of 225 Å (18). Fig. 1 *A* shows the charge distribution of the complete membrane patch without COX as isosurfaces of the electrostatic field at +/− 1 *kT*/e. Although the lipids carry a zero net charge, the membrane exhibits strong inhomogeneities caused by the zwitterionic lipid headgroups. As expected, the inhomogeneities in the external membrane region show a periodicity that reflects the periodic structure of the membrane caused by the construction from identical bilayer patches. In Fig. 1 *B*, the same isosurfaces are displayed, together with the phosphorus and nitrogen atoms of the phosphate and choline groups in the interfacial region of the lipid membrane. It is of interest that the positive (negative) charge distribution does not reflect a major rearrangement of all of the lipids, but results from the presence of an above-average number of nitrogen (phosphorus) groups in the corresponding regions.

Analysis of the BD simulations revealed a large effect of the membrane on the energetics along the association

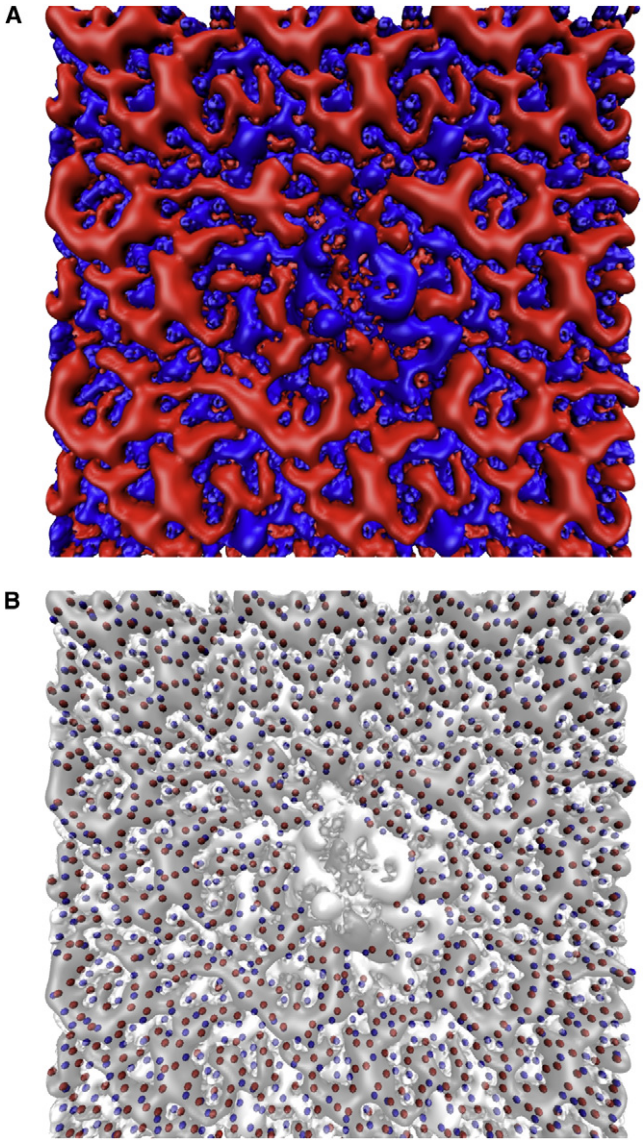

FIGURE 1 Electrostatic field of the DPPC membrane without COX. (*A*) Isosurfaces at +1 *kT*/e (*blue*) and −1 *kT*/e (*red*). Note the three-fold periodicity along the *x* and *y* dimensions that results from the assembly of the lipid patch from eight identical membrane patches. The central box was equilibrated around COX. For calculation of this electrostatic potential map, the COX charges were switched off. (*B*) The same isosurfaces (*white* and *gray*, respectively) and the phosphorus (*red*) and nitrogen (*blue*) atoms of the DPPC headgroups, demonstrating the inhomogeneous charge distribution.

pathway of cytochrome *c*, both cyt c_{552} and cyt c_h, toward COX. Fig. 2, *A* and *B*, shows the energetically favorable regions for the association of cyt c_{552} with fully solvated COX (*blue*), membrane-embedded COX without lipid charges (*green*), and COX embedded in a membrane with lipid charges (*orange*) as isosurfaces of the free-energy landscape at 33% of the corresponding free-energy minimum. In the same manner, Fig. 2, *D* and *E*, displays the results for the association of cyt c_h with COX. These images demonstrate that for both cytochrome *c* species, the energetically favorable regions are very similar for the association with fully solvated COX (*blue*) and with COX embedded in a membrane without lipid charges (*green*). These regions surround subunit II of COX and focus near the Trp^{129} electron entry site. The only noticeable difference is caused by the motional restriction of cytochrome *c* due to the presence of the membrane.

On the other hand, the energetically favorable regions for the association of cytochrome *c* (both cyt c_{552} and cyt c_h) with membrane-embedded COX with full electrostatics not only surround the subunit of COX, but also include several extended patches on the membrane surface. This indicates that cytochrome *c* is attracted by the charge inhomogeneities of the membrane due to the zwitterionic lipid headgroups. To some extent, the patches in the external membrane regions reflect the periodicity of the membrane. Also, the energy and density profiles shown below (see Figs. 4 and 5) support the hypothesis that cytochrome *c* prefers two-dimensional diffusion along the membrane surface over diffusion in free space, though to a different extent, and varying with the ionic strength of the solvent (see below). Furthermore, the patches on the membrane surface for the association of cyt c_{552} and cyt c_h are very similar. Despite the similarity to the inhomogeneities of the electrostatic field, this effect is rather surprising since the inhomogeneities of the electrostatic field of the membrane are on a much smaller length scale than those of the free-energy isosurfaces. Thus, it is most probably the local charge distribution on the membrane caused by the orientations of the lipid headgroups that is complementary to the charge distribution on the surface of cytochrome *c* for specific conformations. To investigate this further, we analyzed the conformations of cyt c_{552} and cyt c_h in these energetically favorable regions. We found that the cyt c_h molecules adopt a preferential orientation close to the membrane. The orientations are very similar for patches corresponding to each other due to the underlying periodicity of the membrane (Fig. 2, *A* and *D*, *two orange patches on left, and two at bottom*). Moreover, the orientations of cyt c_{552} are also similar to the orientations of cyt c_h in these patches.

The free-energy contours displayed in Fig. 2, *A* and *D*, show several minima (corresponding to maxima of the occupancies) at the edges of the lipid bilayer. These minima are probably artifacts caused by edge effects at the boundaries of the lipid leaflet. The lipid slabs were taken from an equilibrated molecular dynamics simulation using periodic boundary conditions. Here, the edges are simply surrounded by a high dielectric region. The shape of the edges therefore does not correspond to a realistic situation. However, one notices that this situation does not create much deeper minima than are found on the membrane surface close to COX. Therefore, we are certain that the computed rates and free-energy contours in the vicinity of COX are not affected by these edge effects.

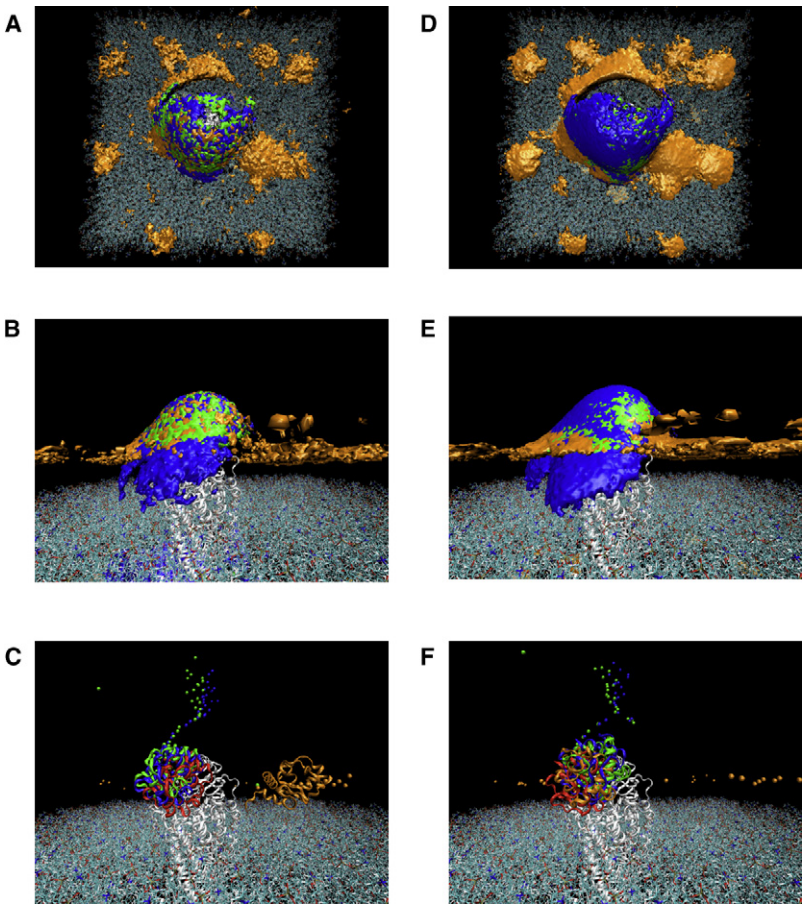

FIGURE 2 Free-energy landscapes and optimal association pathways for cyt c_{552} (*A–C*) and cyt c_h (*D–F*) with COX. (*A*, *B*, *D*, and *E*) Top (*A* and *D*) and side (*B* and *E*) views of free-energy landscapes as isosurfaces at 33% of the corresponding free-energy minimum. Shown are associations of cytochrome *c* with fully solvated COX (*blue*), COX embedded in an uncharged membrane (*green*), and COX embedded in a polar membrane (*orange*). (*C* and *F*) Optimal association pathways and encounter complex conformations, shown as spheres located on the center of mass and as ribbons, respectively. Colors are the same as for isosurfaces. The red ribbon represents cytochrome *c* in the modeled bound conformation.

Fig. 2, *C* and *F*, shows cyt c_{552} and cyt c_h in the encounter complex with COX for the three different scenarios, compared to the bound conformation: fully solvated COX, COX embedded in a completely uncharged membrane, and COX embedded in a polar membrane. As before (26,27), the encounter complex is defined as the state of minimal free energy. For comparison, the bound conformation modeled in a previous docking study (19) is also shown in both images. For both cytochrome *c* species, the position of the encounter state for the association with fully solvated COX and with COX embedded in an uncharged membrane is located very close to the position of the bound state. For the association of cyt c_{552} with fully solvated COX, the encounter complex is very close to the bound state (d_{1-2} = 5.4 Å, RMSD = 5.7 Å), and in the presence of an uncharged membrane, it is a little farther away (9.1 Å and 9.3 Å, respectively). The orientation is also almost the same as in the bound conformation. In the presence of a polar membrane with full electrostatics, however, the encounter state is located on the membrane surface, quite far from the bound structure (d_{1-2} = 53.3 Å, RMSD = 55.9 Å). Conversely, in the case of cyt c_h, only for the association of cyt c_h with fully solvated COX, the orientation is similar to that of the bound structure (d_{1-2} = 9.6 Å, RMSD = 11.1 Å). For the association with membrane-embedded COX (with or without lipid charges), the orientation of the encounter complex is very different, whereas the position is close to that of the bound conformation (for the uncharged membrane, d_{1-2} = 9.4 Å and RMSD = 21.6 Å; for the membrane with lipid charges d_{1-2} = 5.5 Å, RMSD = 22.0 Å).

The positional and orientational distributions of the conformations, i.e., the motional restriction of cytochrome *c* upon association, can be deduced more clearly from the maps of the free-energy landscapes for different membrane environments in Fig. 3, *A* and *B*, for cyt c_{552} and in Fig. 3, *C* and *D*, for cyt c_h. In these maps, the free-energy landscape is shown for all conformations with a free energy of at least 96% of the corresponding free-energy minimum. The maps underline that the position of cyt c_{552} in the encounter state is very close to that of the docking model for the bound state for the association with fully solvated COX and in the presence of an uncharged membrane (Fig. 3 *A*). The average orientation in both cases is close to that of the bound structure, but the distribution is rather dispersed (Fig. 3 *B*). More precisely, the normal vectors in these cases are centered around 3.3° ± 7.0°, and 2.7° ± 6.5°, measured between the normal vectors on the interface patches of the encounter-state conformations and that of the bound state. For membrane-embedded COX with full electrostatics, the

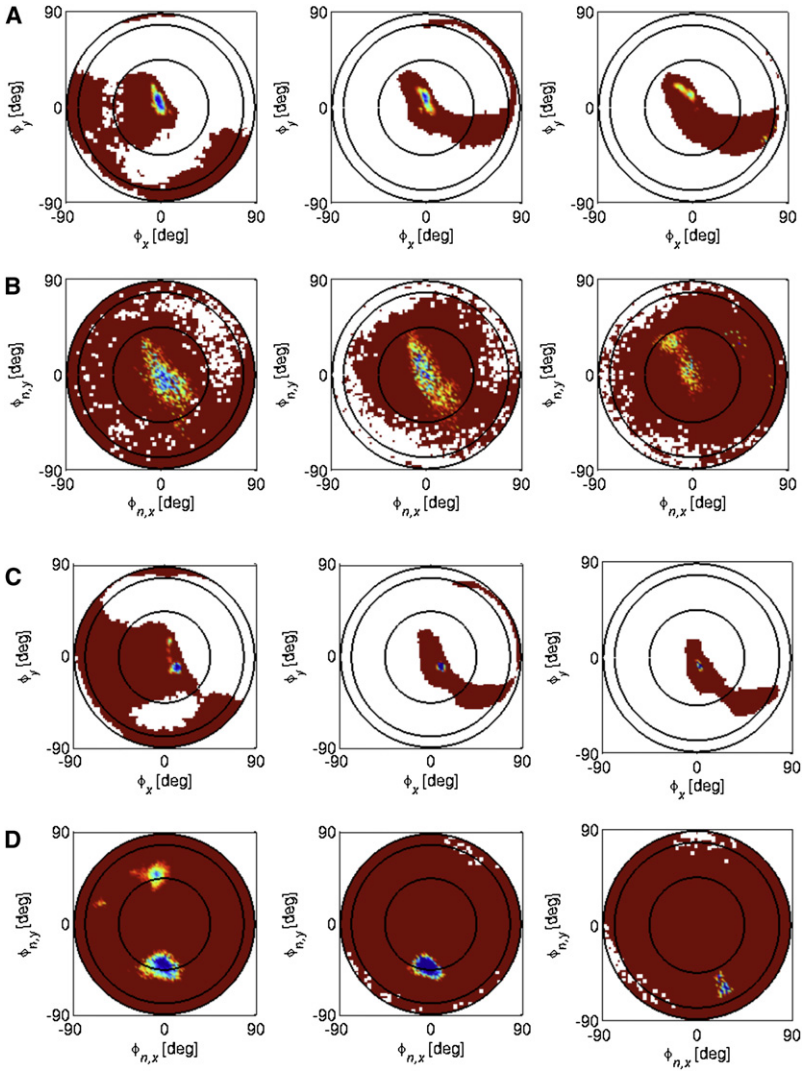

FIGURE 3 Free-energy landscape maps for the energetically most favorable conformations of cyt c_{552} (*A* and *B*) and cyt c_h (*C* and *D*) with COX. Maps for positional and orientational coordinates for the association of cytochrome *c* with fully solvated COX (*left*), COX embedded in a membrane without lipid charges (*center*); and COX embedded in a membrane with full electrostatics (*right*). Free energy levels range from low (*blue*) to high (*red*) (*A* and *C*) Translational free-energy landscapes. (*B* and *D*) Orientational free-energy landscapes.

orientation of cyt c_{552} is rotated (19.0° ± 24.8°) due to the larger distance from the bound state. For cyt c_h, the positions in all three cases are slightly shifted, but the distribution of the normal vectors is more focused. In all cases (fully solvated COX, and COX embedded in an uncharged membrane and in a charged membrane), the most favorable orientation is found in the lower part of the maps at around 30° or more from the normal vector in the ''bound'' state. For fully solvated COX, the normal vectors can also be located in a second region, again at 30°, but in the upper part. This gives rise to a larger standard deviation (23.3° ± 16.6°) compared to membrane-embedded COX (28.4° ± 5.7° without electrostatics, and 43.1° ± 4.5° with electrostatics). As the ''bound'' conformations of cytochrome *c* were inferred from the docking study (19), this result indicates that during the simulated trajectories, cyt c_{552} converges toward the docked conformation when encountering COX, whereas cyt c_h converges toward a conformation that is rotated at around 30° with respect to its docked conformation.

Fig. 4 shows the energy profiles for the association of cyt c_{552} and cyt c_h with fully solvated COX, with COX embedded in a membrane without lipid charges, and with COX embedded in a membrane with full electrostatics. To estimate the statistical error in these energy profiles, we ran the simulation of cyt c_{552} and COX embedded in a polar membrane for five different sets of random numbers. The corresponding profiles for this setup are shown as averages, with the standard deviation as error bars. The free-energy profiles from the simulations of cytochrome *c* (both cyt c_{552} and cyt c_h) association with COX are very similar in the case of fully solvated COX and COX embedded in an uncharged membrane, whereas the presence of a polar membrane has two main effects on the free-energy profiles. The first is a slight, but systematic, variation of the free energy in the encounter state. This can be understood as an enhancement of the charge complementarity of the proteins due to the presence of the membrane. In the case of cyt c_{552}, this means a slightly decreased depth of the free-energy minimum from −7.50 kcal/mol for fully solvated COX to

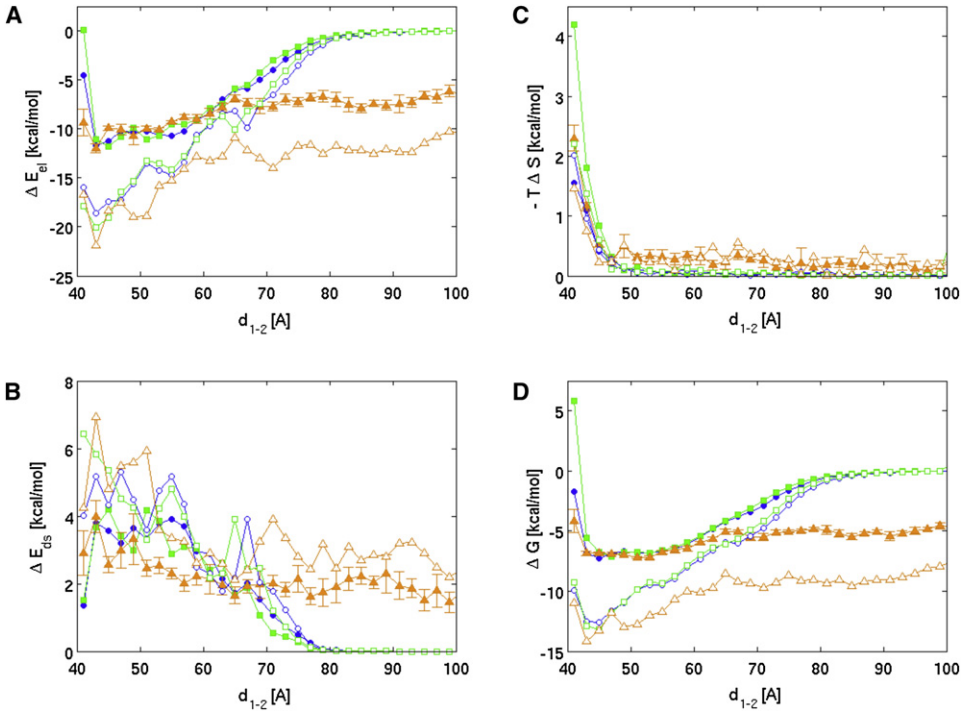

FIGURE 4 Energy profiles along minimal free-energy pathways. Effects of the membrane on the energy profiles are shown for cyt c_{552} (*solid symbols*) and cyt c_h (*open symbols*) with COX (200 mM). The energies are displayed with respect to the distance between protein centers for three different association scenarios for cytochrome *c*: with fully solvated COX, with COX embedded in an uncharged membrane, and with COX embedded in a polar membrane. The color scheme is the same as for Fig. 2. (*A*) Electrostatic energy, ΔE_{el}; (*B*) Desolvation energy, ΔE_{ds}; (*C*) Translational/rotational entropy loss, $-T\Delta S$. (*D*) Free energy, ΔG. The profiles for cyt c_{552} with COX embedded in a polar membrane are mean values with corresponding standard deviations from five simulations.

−7.26 kcal/mol for COX embedded in the partially charged membrane. In contrast to the negative charge of cyt c_{552}, cyt c_h has a large positive charge, and since COX carries a large negative charge, the depth of the free-energy minimum is increased, from −12.93 kcal/mol for fully solvated COX to −14.30 kcal/mol for membrane-embedded COX.

The second effect of the polar membrane gets visible for larger protein separations. Both cyt c_{552} and cyt c_h are attracted by the inhomogeneous charge distribution caused by the polar lipid headgroups. The free energy for cyt c_{552} localized near the membrane is lowered by ~5 kcal/mol compared to localization far from the membrane (and COX). For cyt c_h, this attraction is even stronger, up to 10 kcal/mol. When located near to the favorable binding areas on the membrane surface, the rotational freedom of cyt c_h is reduced, as shown in Fig. 3.

To investigate the effect of the membrane more precisely, we also analyzed the occupancy landscape for the association of cytochrome *c* with COX. Fig. 5 shows the density profiles along the *z* axis, which were computed by integrating the occupancies in the *x* and *y* directions and normalized to the total occupancy in the interval between $z = 0$ and $z = 100$ Å. To exclude the immediate effect of COX, all the occupancies within a radius of 40 Å in the *xy* direction were ignored in these calculations. At an ionic strength of 200 mM (Fig. 5 *A*), we found no striking difference for the association of cyt c_{552} to COX embedded in an uncharged or polar membrane, or to uncharged COX embedded in a polar membrane. On the contrary, for cyt c_h, the close vicinity of the membrane is increasingly attractive for a polar membrane, even with uncharged COX. The presence of a 20% negatively charged membrane is very attractive for both cytochrome *c* species, and the peak in the density profile shifts to ~42 Å. This effect is rather huge for cyt c_h, indicating that in this setup it diffuses basically in two dimensions, and the occupancy farther away from the membrane decreases significantly.

We computed the average lifetimes for cyt c_{552} and cyt c_h in the interval $z = 40$–50 Å. On the whole, they reflect the effects seen in the density profiles: For cyt c_{552}, the lifetime varies only slightly for the association with solvated COX (46.6 ps), COX embedded in an uncharged membrane (50.9 ps), and COX embedded in a polar membrane (48.6 ps). On the contrary, for cyt c_h it increases from 50.0 ps for solvated COX to 56.6 ps for COX embedded in an uncharged membrane and to 63.2 ps for COX embedded in a polar membrane. For COX embedded in a 20% negatively charged membrane, the lifetime slightly decreased to 45.1 ps for cyt c_{552}, whereas it increased significantly, to 85.9 ps, for cyt c_h. Due to the shift of the peak in the density profiles, in this setup, the lifetime was calculated for the interval $z = 37$–47 Å.

Whether the membrane lipids are able to respond to the presence of the protein by reorienting their headgroups should be judged based on a comparison of the corresponding timescales for transient protein binding to the membrane and for lipid motions. The typical timescale for lipid headgroup rotations or lipid protrusions is in the range of nanoseconds (43–45). The realistic timescale for protein binding, however, will be longer than the residence times computed above because of the missing short-range interactions. Properly accounting for them would clearly increase the average

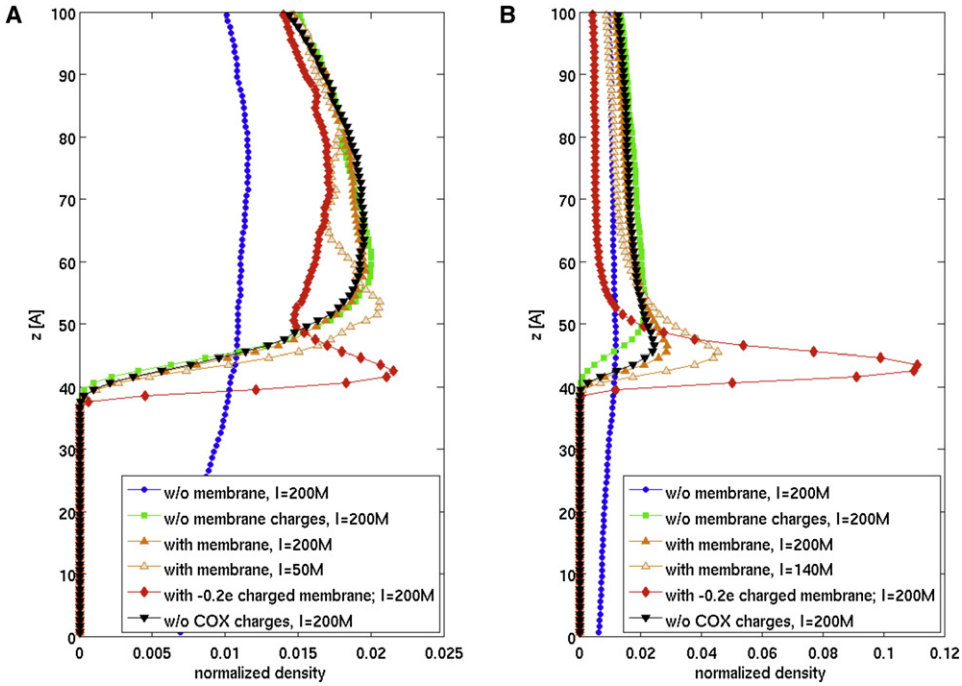

FIGURE 5 Density profiles along the z axis. The effects of the membrane on the density profiles for the association of cyt c_{552} (*A*) and cyt c_h (*B*) with COX. The profiles are normalized to the total occupancy in the interval $z = 0$–100 Å, and all occupancies within a radius of 40 Å in the xy direction around the COX center were omitted to exclude the immediate effect of COX.

lifetimes of cytochrome *c*. In addition, given a flexible representation of the membrane lipids, the lipids would be able to respond to the presence of the protein to increase the attractive interaction. Altogether, it is reasonable to assume similar timescales of protein association and of lipid headgroup rotations so that the lipids are able to respond to the electrostatic field of the protein like a viscous liquid, and the attractive patches remain intact as long as the diffusing protein is close by.

In our previous study (18), we analyzed the association rates of cyt c_{552} and cyt c_h with COX. Since cyt c_h carries a much higher and electrostatically complementary charge than cyt c_{552}, the computed relative rates between the two cytochrome *c* species and COX differ roughly by one magnitude, which corresponds particularly well to the experimental data (9,10). Compared to the association with fully solvated COX, the presence of the uncharged membrane decreased the association rates slightly. This result indicates a slightly unfavorable role of such a steric obstacle. Switching on the partial charges of the membrane lipids had no large effects on the computed rates. At close inspection, we noted that the partial charges increased the rate for the physiological partner cyt c_{552} slightly, whereas they decreased the rate for cyt c_h.

Effects of different redox states

Besides the effects of the membrane on the association behavior of cytochrome *c* with COX, we also investigated the effects of different redox states of cyt c_{552} and membrane-embedded COX. Fig. 6 illustrates the effect of the electron transfer from cyt c_{552} to completely oxidized COX, and to COX oxidized only at the Cu_A center. In particular, Fig. 6 *A* presents the free-energy profiles for the association process for both configurations before and after the transfer of the electron. The figure shows that the free-energy minimum of the encounter state is less favorable before the electron transfer than after the transfer, and, furthermore, that the encounter state is much closer to the bound state after the electron transfer. This is a rather counterintuitive result, as one might imagine the electron transfer to have a destabilizing effect on the complex to enable the dissociation of cytochrome *c*. For the same reason, one may assume that association of oxidized cyt c_{552} should be favored over the approach of the reduced species. However, the computed rates in Fig. 6 *B* for cyt c_{552} and COX in the different oxidation states reveal exactly the opposite behavior. On second thoughts, however, this result can be easily understood. Electron transfer makes the overall charge of cyt c_{552} more positive and enhances the electrostatic complementarity of both proteins. Therefore, the effects on the free energy profiles and on the association rates can be explained by the increased charge complementarity between the proteins due to the electron transfer. These results are very similar for the two scenarios, the electron transfer to completely oxidized COX and to three-times-reduced COX; the differences in the free energy before and after the electron transfer are also quite close. Only the absolute values of the free energy in the encounter states are slightly higher for the association with completely oxidized COX.

DISCUSSION

In the BD simulations performed, we found a prominent effect of the membrane on the association of cytochrome *c* to COX. For the simulation of membrane-embedded COX, we used

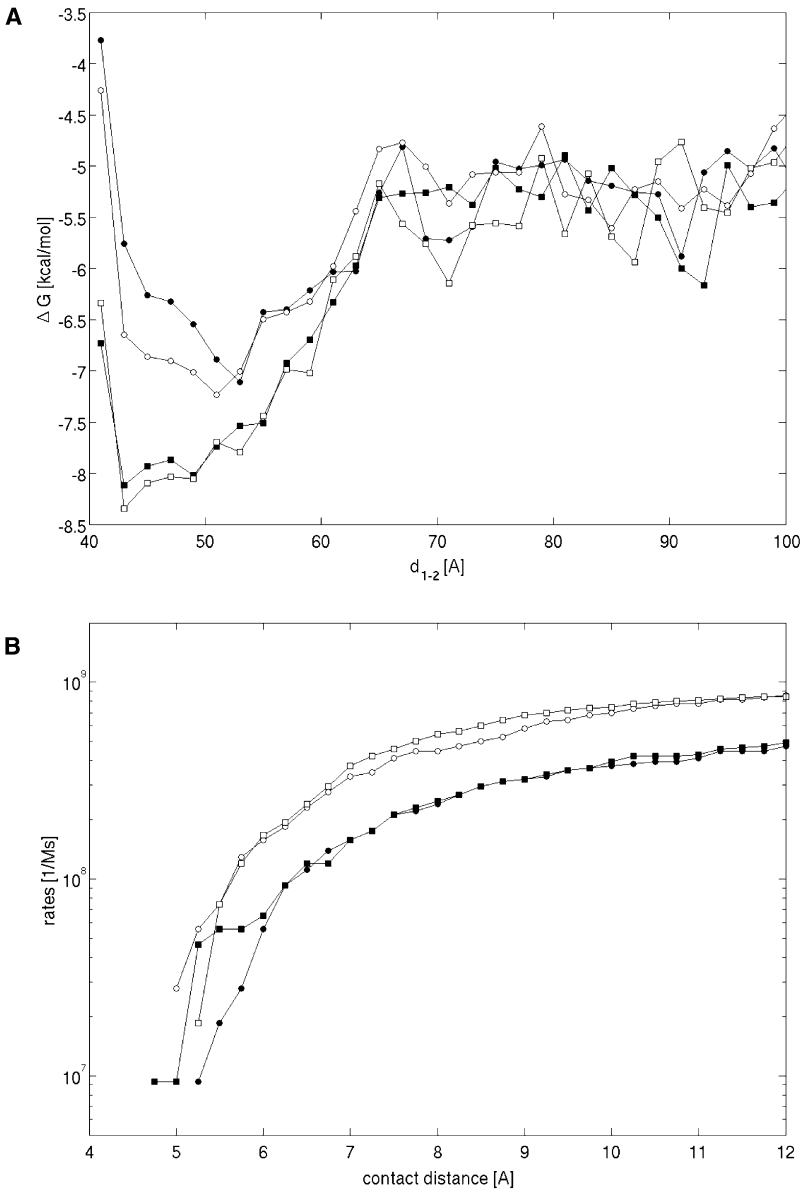

FIGURE 6 Free-energy profiles along minimal free-energy pathways (*A*) and computed association rates (*B*). The effects are shown of different redox states on (*A*) the free-energy profile and (*B*) the association rates for cyt c_{552} and membrane-embedded COX (with full electrostatics). The plots show the results from simulations of reduced cyt c_{552} to fully oxidized COX (*solid squares*) and to COX only oxidized at the Cu_A center (*solid circles*), and from simulations of oxidized cyt c_{552} to fully reduced COX (*open circles*) and to COX only reduced at the Cu_A center (*open squares*).

a snapshot of an atomistically modeled large square DPPC membrane patch from a molecular dynamics study. On the one hand, it is clear that this snapshot only represents one particular conformation of the lipid molecules at a certain point in time. On the other hand, it appears more realistic than a time-averaged conformation of the lipid membrane, since it shows the inhomogeneities of the electrostatic field of the membrane. By analyzing the free-energy landscape and the energy profiles, we found that these particular inhomogeneities, which are caused by the arrangement of the lipid headgroups, are responsible for the attraction between cytochrome *c* and the lipid membrane. In addition, we found a strong correlation of the regions of minimal free energy on the membrane and the orientation of cytochrome *c*. With the assumption that the lipids are able to respond to the electrostatic field of cytochrome *c*, we conclude that cytochrome *c* diffuses parallel to the membrane rather than in three dimensions. This effect is enhanced for cyt c_h as compared to cyt c_{552} and is stronger for lower ionic strength. This behavior was also found experimentally for cyt c_h at low ionic strengths (23). In the presence of a 20% negatively charged membrane, cyt c_h practically diffuses only laterally on the membrane surface.

Due to the attractive interaction of cytochrome *c* with a polar membrane, the free energy also for large distances is strongly decreased compared to fully solvated COX or COX embedded in an uncharged membrane. This leads to a very flat free-energy minimum since the free energy in the encounter state is not significantly different for fully solvated COX and membrane-embedded COX (uncharged or polar membrane). Therefore, the encounter complex for COX embedded in a polar membrane is not as well defined

as in the case of fully solvated COX or COX embedded in an uncharged membrane, or as in the previous studies on the barnase/barstar system (27).

With the assumption of a lateral diffusion of cytochrome *c* on the surface of a polar or charged membrane, however, one would expect a larger effect on the association rates. But here, as mentioned above, it is questionable whether the membrane snapshot describes the experimental setup correctly. Due to the missing response of the membrane lipids to the electrostatic field of the protein, cytochrome *c* has to ''jump'' between the ''islands'' (patches) of favorable free energy on the membrane surface to encounter COX. Thus, cytochrome *c* cannot profit from the attractive patches on the membrane surface, and therefore, the rates are not significantly altered.

Analyzing the motional restrictions of cyt c_{552} and cyt c_h in the encounter states showed that the conformation of cyt c_{552} in this state is very close to that of the docking model, whereas cyt c_h appears to be rotated ~30° relative to this conformation. A similar rotation was observed in our previous study on the barnase/barstar complex (27). We suggest that long-range attraction to the encounter complex and formation of short-range contacts during the transition from encounter to bound complex may be mediated by different regions on the two protein surfaces. Therefore, it appears quite reasonable that the proteins may adapt different orientations in the encounter and bound states.

By studying the effects of different redox states on the association behavior of cyt c_{552} and membrane-embedded COX, we found that the interaction between these proteins is more attractive after the electron transfer. This can be explained by the increased charge complementarity between the proteins due to the electron transfer. For the interpretation of these results, one should keep in mind, though, that the rigid-body approximation used in Brownian dynamics simulations may provide an incorrect picture of the binding energetics before and after electron transfer (Figs. 5 *B* and 6). It is commonly assumed that long-range forces are the driving forces for the association kinetics (k_{on} rates) and short-range forces are the dominant effects for the dissociation kinetics (k_{off} rates). Upon binding, short-range contacts, such as hydrogen bonds, and tight-packing contacts are formed. These are probably of much greater importance than the net change of total charges noted above. Nonetheless, it is interesting to note that the transfer of a net charge counteracts the polarity of the binding partners.

In summary, Brownian dynamics simulations have enabled us to provide a new spatial view of the association pathways of the electron carrier with the terminal oxidase in mitochondria, cytochrome *c* oxidase. The results of the simulation provide new support for the previously suggested model of two-dimensional diffusion along the lipid bilayer. For the association of cytochrome *c* and COX in the biological cell, this means that this process is strongly influenced by the composition of the lipid membrane and the presence of other membrane proteins. Furthermore, we therefore conclude that experiments with soluble COX do not appear to be directly comparable to the native membrane environment. Based on our studies, we suggest that normal fluctuations in the lipid distribution cause temporal favorable binding sites on the membrane surface. This study calls for an extension of future work using a dynamic description of the membrane. As described, for example, by Heimburg et al. (46), the membrane lipids are likely to respond to the presence of a bound macromolecule. As the positions of the residues on the surface of the protein are quite well defined, it is the lipids that need to reorganize. In light of this study, we suggest that the lipids are rearranged to create a sort of negative image of the protein surface. On the other hand, one can also imagine slight penetration of cytochrome *c* into the headgroup region due to the fluid nature of membranes. Treating the energetic and structural details of protein/membrane interactions is becoming within reach of molecular simulation methods involving Brownian dynamics, molecular dynamics, Monte Carlo simulations, and other techniques, as, e.g., presented by Kelashvili et al. (47). By interfacing with time-resolved or single-molecule experiments, we can expect to understand much more about these fascinating systems in the near future.

We gratefully acknowledge financial support from the Deutsche Forschungsgemeinschaft via the Center for Bioinformatics in Saarbrücken. A.S. gratefully acknowledges financial support from the Deutsche Forschungsgemeinschaft for a research fellowship (SP 1104/1-1). We thank Michael Hutter for helpful discussions, Rebecca C. Wade (European Molecular Biology Laboratory, Heidelberg, Germany) for providing the SDA software package and comments on the manuscript, Elena Olkhova (Max Planck Institute of Biophysics, Frankfurt, Germany) for comments on the manuscript, and Christopher P. Berrie (Consorzio Mario Negri Sud, Santa Maria Imbaro (Chieti), Italy) for editorial assistance.

REFERENCES

1. Farver, O., E. Grell, B. Ludwig, H. Michel, and I. Pecht. 2006. Rates and equilibrium of Cu_A to heme a electron transfer in *Paracoccus denitrificans* cytochrome *c* oxidase. *Biophys. J.* 90:2131–2137.
2. Witt, H., F. Malatesta, F. Nicoletti, M. Brunori, and B. Ludwig. 1998. Tryptophan 121 of subunit II is the electron entry site to cytochrome-c oxidase in *Paracoccus denitrificans*. *J. Biol. Chem.* 273:5132–5136.
3. Belevich, I., M. I. Verkhovsky, and M. Wikström. 2006. Proton-coupled electron transfer drives the proton pump of cytochrome *c* oxidase. *Nature*. 440:829–832.
4. Michel, H. 1999. Cytochrome *c* oxidase: catalytic cycle and mechanisms of proton pumping–a discussion. *Biochemistry*. 38:15129–15140.
5. Tang, C., J. Iwahara, and G. M. Clore. 2006. Visualization of transient encounter complexes in protein–protein association. *Nature*. 444:383–386.
6. Gabdoulline, R. R., and R. C. Wade. 1997. Simulation of the diffusional association of barnase and barstar. *Biophys. J.* 72:1917–1929.
7. Elcock, A. H., R. R. Gabdoulline, R. C. Wade, and J. A. McCammon. 1999. Computer simulation of protein-protein association kinetics: acetylcholinesterase-fasciculin. *J. Mol. Biol.* 291:149–162.
8. Madura, J. D., J. M. Briggs, R. C. Wade, M. E. Davis, B. A. Luty, et al. 1995. Electrostatics and diffusion in solution: simulations with the

University of Houston Brownian Dynamics Program. *Comput. Phys. Commun.* 91:57–95.

9. Drosou, V., F. Malatesta, and B. Ludwig. 2002. Mutations in the docking site for cytochrome *c* on the *Paracoccus* heme aa_3 oxidase: electron entry and kinetic phases of the reaction. *Eur. J. Biochem.* 269:2980–2988.
10. Maneg, O., B. Ludwig, and R. Malatesta. 2003. Different interaction modes of two cytochrome *c* oxidase soluble Cu_A fragments with their subtrates. *J. Biol. Chem.* 278:46734–46740.
11. Gabdoulline, R. R., and R. C. Wade. 2001. Protein-protein association: investigation of factors influencing association rates by Brownian dynamics simulation. *J. Mol. Biol.* 306:1139–1155.
12. Autenrieth, F., E. Tajkhorshid, K. Schulten, and Z. Luthey-Schulten. 2004. Role of water in transient cytochrome c_2 docking. *J. Phys. Chem. B.* 108:20376–20387.
13. Miyashita, O., M. Y. Okamura, and J. N. Onuchic. 2003. Theoretical understanding of the interprotein electron transfer between cytochrome c_2 and the photosynthetic reaction center. *J. Phys. Chem. B.* 107: 1230–1241.
14. Miyashita, O., J. N. Onuchic, and M. Y. Okamura. 2003. Continuum electrostatic model for the binding of cytochrome c2 to the photosynthetic reaction center from *Rhodobacter sphaeroides*. *Biochemistry.* 42:11651–11660.
15. Miyashita, O., J. N. Onuchic, and M. Y. Okamura. 2004. Transition state and encounter complex for fast association of cytochrome c_2 with bacterial reaction center. *Proc. Natl. Acad. Sci. USA.* 101:16174–16179.
16. Mulgrew-Nesbitt, A., K. Diraviyam, J. Wang, S. Singh, P. Murray, et al. 2006. The role of electrostatics in protein-membrane interactions. *Biochim. Biophys. Acta.* 1761:812–826.
17. Murray, D., A. Arbuzova, G. Mihaly, A. Gambir, N. Ben-Tal, et al. 1999. Electrostatic properties of membranes containing acidic lipids and adsorbed basic peptides. Theory and experiment. *Biophys. J.* 77:3176–3188.
18. Flöck, D., and V. Helms. 2004. A Brownian dynamics study: the effect of a membrane environment on an electron transfer system. *Biophys. J.* 87:65–74.
19. Flöck, D., and V. Helms. 2002. Protein-protein docking of electron transfer complexes: cytochrome c oxidase and cytochrome c. *Proteins.* 47:75–85.
20. Wienk, H., O. Maneg, C. Lücke, P. Pristovsek, F. Löhr, et al. 2003. Interaction of cytochrome c with cytochrome c oxidase: an NMR study on two soluble fragments derived from *Paracoccus denitrificans*. *Biochemistry.* 42:6005–6012.
21. Maneg, O., F. Malatesta, B. Ludwig, and V. Drosou. 2004. Interaction of cytochrome *c* with cytochrome oxidase: two different docking scenarios. *Biochim. Biophys. Acta.* 1655:274–281.
22. Bertini, I., G. Cavallaro, and A. Rosato. 2005. A structural model for the adduct between cytochrome *c* and cytochrome *c* oxidase. *J. Biol. Inorg. Chem.* 10:613–624.
23. Gupte, S. S., and C. R. Hackenbrock. 1988. Multidimensional diffusion modes and collision frequencies of cytochrome c with its redox partners. *J. Biol. Chem.* 263:5241–5247.
24. Krab, K., M. J. Wagner, A. M. Wagner, and I. M. Møller. 2000. Identification of the site where the electron transfer chain of plant mitochondria is stimulated by electrostatic charge screening. *Eur. J. Biochem.* 267:869–876.
25. Gorba, C., T. Geyer, and V. Helms. 2004. Brownian dynamics simulations of simplified cytochrome *c* molecules in the presence of a charged surface. *J. Chem. Phys.* 121:457–464.
26. Spaar, A., and V. Helms. 2005. Free energy landscape of protein-protein encounter resulting from Brownian dynamics simulations of barnase:-barstar. *Barstar. J. Chem. Theory Comput.* 1:723–736.
27. Spaar, A., C. Dammer, R. R. Gabdoulline, R. C. Wade, and V. Helms. 2006. Diffusional encounter of barnase and barstar. *Biophys. J.* 90:1913–1924.
28. Ostermeier, C., A. Harrenga, U. Ermler, and H. Michel. 1997. Structure at 2.7 Å resolution of the *Paracoccus denitrificans* two-subunit cytochrome *c* oxidase complexed with an antibody F-V fragment. *Proc. Natl. Acad. Sci. USA.* 94:10547–10553.
29. Harrenga, A., B. Reincke, H. Ruterjans, B. Ludwig, and H. Michel. 2000. Structure of the soluble domain c_{522} from *Paracoccus denitrificans* in the oxidized and reduced states. *J. Mol. Biol.* 295:667–678.
30. Bushnell, G. W., G. V. Louie, and G. D. Brayer. 1990. High-resolution three-dimensional structure of horse heart cytochrome c. *J. Mol. Biol.* 214:585–595.
31. Olkhova, E., V. Helms, and H. Michel. 2005. Titration behavior of residues at the entrance of the D-pathway of cytochrome *c* oxidase from *Paracoccus denitrificans* investigated by continuum electrostatic calculations. *Biophys. J.* 89:2324–2331.
32. Davis, M. E., J. D. Madura, B. A. Luty, and J. A. McCammon. 1991. Electrostatic and diffusion of molecules in solution: simulations with the University-of-Houston-Brownian dynamics program. *Comput. Phys. Commun.* 62:187–197.
33. Case, D. A., T. E. Cheatham, T. Darden, H. Gohlke, R. Luo, et al. 2005. The Amber biomolecular simulation programs. *J. Comput. Chem.* 26:1668–1688.
34. Gabdoulline, R. R., and R. C. Wade. 1996. Effective charges for macromolecules in solvent. *J. Phys. Chem.* 100:3868–3878.
35. Northrup, S. H., J. O. Boles, and J. C. L. Reynolds. 1987. Electrostatic effects in the Brownian dynamics of association and orientation of heme proteins. *J. Phys. Chem.* 91:5991–5998.
36. Gabdoulline, R. R., and R. C. Wade. 1998. Brownian dynamics simulation of protein-protein diffusional encounter. *Methods.* 14:329–341.
37. Northrup, S. H., and H. P. Erickson. 1992. Kinetics of protein-protein association explained by Brownian dynamics computer simulation. *Proc. Natl. Acad. Sci. USA.* 89:3338–3342.
38. Ermak, D. L., and J. A. McCammon. 1978. Brownian dynamics with hydrodynamic interactions. *J. Chem. Phys.* 69:1352–1360.
39. Eltis, L. D., R. E. Herbert, P. D. Barker, A. G. Mauk, and S. H. Northrup. 1991. Reduction of horse heart ferricytochrome *c* by bovine liver ferrocytochrome b5. *Biochemistry.* 30:3663–3674.
40. Antosiewicz, J., J. M. Briggs, and J. A. McCammon. 1996. Orientational steering in enzyme-substrate association: ionic strength dependence of hydrodynamic torque effects. *Eur. Biophys. J.* 24:137–141.
41. Tidor, B., and M. Karplus. 1994. The contribution of vibrational entropy to molecular association. The dimerization of insulin. *J. Mol. Biol.* 238:405–414.
42. Yeung, T., G. E. Gilbert, J. Shi, J. Silvius, A. Kapus, et al. 2008. Membrane phosphatidylserine regulates surface charge and protein localization. *Science.* 319:210–213.
43. Klauda, J. B., M. F. Roberts, A. G. Redfield, B. R. Brooks, and R. W. Pastor. 2008. Rotation of lipids in membranes: molecular dynamics simulation, 31P spin-lattice relaxation, and rigid-body dynamics. *Biophys. J.* 94:3074–3083.
44. Böckmann, R. A., and H. Grubmüller. 2004. Multistep binding of bivalent cations to phospholipid bilayers: a molecular dynamics study. *Angew. Chem. Int. Ed.* 43:1021–1024.
45. Böckmann, R. A., B. L. de Groot, S. Kakorin, E. Neumann, and H. Grubmüller. 2008. Kinetics, statistics, and energetics of lipid membrane erlectroporation studied by molecular dynamics simulations. *Biophys. J.* 95:1837–1850.
46. Heimburg, T., B. Angerstein, and D. Marsh. 1999. Binding of peripheral proteins to mixed lipid membranes: The effect of local demixing upon binding. *Biophys. J.* 76:2575–2586.
47. Khelashvili, G., H. Weinstein, and D. Harries. 2008. Protein diffusion on charged membranes: a dynamic mean-field model describes time evolution and lipid reorganization. *Biophys. J.* 94:2580–2597.